Available online at www.sciencedirect.com
ScienceDirect
Trans. Nonferrous Met. Soc. China 19(2009) 99−107
Transactions of Nonferrous Metals Society of China
www.tnmsc.cn

Comparison of thermal shock behaviors between plasma-sprayed nanostructured and conventional zirconia thermal barrier coatings

LIU Chun-bo(刘纯波)[1], ZHANG Zhi-min(张志民)[1], JIANG Xian-liang(蒋显亮)[1],
LIU Min(刘 敏)[2], ZHU Zhao-hui(朱朝辉)[2]

1. School of Materials Science and Engineering, Central South University, Changsha 410083, China;
2. Guangzhou Research Institute of Nonferrous Metals, Guangzhou 510651, China

Received 3 January 2008; accepted 28 April 2008

Abstract: NiCoCrAlTaY bond coat was deposited on pure nickel substrate by low pressure plasma spraying(LPPS), and ZrO_2-8%Y_2O_3 (mass fraction) nanostructured and ZrO_2-7%Y_2O_3 (mass fraction) conventional thermal barrier coatings(TBCs) were deposited by air plasma spraying(APS). The thermal shock behaviors of the nanostructured and conventional TBCs were investigated by quenching the coating samples in cold water from 1 150, 1 200 and 1 250 ℃, respectively. Scanning electron microscopy(SEM) was used to examine the microstructures of the samples after thermal shock testing. Energy dispersive analysis of X-ray(EDAX) was used to analyze the interface diffusion behavior of the bond coat elements. X-ray diffractometry(XRD) was used to analyze the constituent phases of the samples. Experimental results indicate that the nanostructured TBC is superior to the conventional TBC in thermal shock performance. Both the nanostructured and conventional TBCs fail along the bond coat/substrate interface. The constituent phase of the as-sprayed conventional TBC is diffusionless-transformed tetragonal(t'). However, the constituent phase of the as-sprayed nanostructured TBC is cubic(c). There is a difference in the crystal size at the spalled surfaces of the nanostructured and conventional TBCs. The constituent phases of the spalled surfaces are mainly composed of $Ni_{2.88}Cr_{1.12}$ and oxides of bond coat elements.

Key words: nanocrystalline zirconia; plasma spray; thermal barrier coating; thermal shock test; coating failure

1 Introduction

Thermal barrier coatings(TBCs) have been widely applied to hot section components of gas turbine engines, such as blade and combustion chamber[1−2]. Over the past ten years, nanostructured zirconia TBCs have become a hot research field. New coating systems with addition of rare earth oxides are developed[3−4]. Nanostructured zirconia TBC exhibits improved wear-resistance, thermal shock resistance and thermal insulation capability, due to the modification of its structure[5−10]. However, TBCs spall or debond under high-temperature thermal cycling conditions. Thus, thermal shock behavior is an important indication of TBCs performance. Thermal shock failure results from the stress generated during TBCs service, mainly affected by coating thickness, phase constituent, deposition temperature, oxidation and surface roughness of bond coat, and service environment[11−15]. Conventional TBC spalls directly from bond coat due to the lack of stress relief during thermal cycling. In recent years, the thermal shock performance of nanostructured zirconia TBC has been reported. The test result indicated that the nanostructured TBC deposited by air plasma spraying(APS) of ZrO_2-5%Y_2O_3 (molar fraction) nanocrystalline powder had good thermal shock performance in vacuum[16]. After water quenching from high temperatures, the APS nanostructured TBC failed mainly between two vertical cracks in the top coat[12]. The thermal shock performance of the nanostructured TBC was enhanced, because it had high porosity and uniform pore distribution without penetrating and parallel cracks and monoclinic phase[17]. The stress is the main reason for explaining the life difference between the nanostructured and conventional TBCs. The finite element method was employed to analyze the stress distribution in the APS nanostructured and conventional TBCs during thermal cycling process. The calculation result indicated that the stress within the

Foundation item: Project(1343-77212) supported by the Innovation Program for Graduate Students of Central South University, China
Corresponding author: JIANG Xian-liang; Tel: +86-731-8876307; E-mail: xljiang@mail.csu.edu.cn
DOI: 10.1016/S1003-6326(08)60235-6

nanostructured TBC in the axial direction was about 67% that of the conventional TBC; the stress in the radial direction at the vicinity of the interface between thermally grown oxide (TGO) and top coat at the edge of the TBC samples was only about 73% that of the conventional TBC[18].

The objective of this investigation is to examine the coating structure, constituent phases of zirconia top coat, interface diffusion behavior of bond coat elements, morphology and constituent phases of the spalled surface of APS nanostructured TBC after thermal shock testing, using conventional TBC for the purpose of comparison. Complete understanding of the thermal shock failure mechanism of nanostuctured TBC will be important in enhancing the serving life of nanostructured TBCs.

2 Experimental

2.1 Sample preparation

Original nanocrystalline zirconia powder was purchased from Yisite Patent Technologies Development Company, Shijiazhuang, China. Its nominal composition is ZrO_2-8%Y_2O_3 (mass fraction). Its grain size is 25 nm. Because of the poor flow ability of the original nanocrystalline powder that was unsuitable for plasma spraying, the original nanocrystalline powder was agglomerated by spray drying in Hunan Bestful Materials Limited Corporation, Changsha, China. The spray-dried powder was heat-treated in air at 1 250 ℃ for 2 h. Spherical and donut-like agglomerated particles were obtained after the spray drying and heat treatment. Particle size distribution of the heat-treated, agglomerated nano-powder is in the range of 10−40 μm. Conventional powder feedstock is a commercial powder with the composition of ZrO_2-7%Y_2O_3 (mass fraction). This is a fused and crushed powder. Particle size distribution of the conventional powder is in the range of 10−80 μm. The composition of bond coat is Ni-23Co-20Cr-9Al-4.2Ta-0.6Y (mass fraction, %). Pure nickel was used as substrate with a dimension of 60 mm×30 mm×2 mm.

Plasma spray experiments were conducted in the Guangzhou Research Institute of Nonferrous Metals, China. APS facility used is MP−P−1500 model made by GTV Corporation, Germany. APS parameters for depositing nanostructured and conventional zirconia TBCs are given in Table 1. Nanostructured zirconia TBC thickness was 150−200 μm. Conventional zirconia TBC thickness was about 220 μm. The bond coat was deposited on the nickel substrate by low pressure plasma spraying(LPPS). LPPS facility used is JZJH−600 model. Bond coat thickness was about 100 μm. The bond coat was deposited for both the nanostructured and conventional TBCs.

Table 1 Air plasma spray parameters for depositing nanostructured and conventional zirconia TBCs

Plasma power/ kW	Spray distance/ mm	Powder feed rate/ ($g\cdot min^{-1}$)	Ar flow rate/ ($L\cdot min^{-1}$)	H_2 flow rate/ ($L\cdot min^{-1}$)
40	100	10-40	40	5

2.2 Thermal shock test

The thermal shock test was performed by water quenching method. Three pieces of the nanostructured TBC sample were put in one zirconia crucible and 2 pieces of the conventional TBC sample were put in another crucible before thermal shock testing each time. The samples were heated in SX_2−10−13 box furnace (Experimental Furnace Factory of Changsha, China) in air for 30 min at 1 150, 1 200 and 1 250 ℃, respectively, and then quenched into ambient water with 25 ℃ for 10 min. Spallation with more than 50% of the total area of the zirconia top coat was adopted as the criteria for coating failure. The number of thermal cycles was recorded.

2.3 Coating characterization

TBC samples were mounted in epoxy resin and polished first by grit papers and then by polishing cloth. The microstructure and elements distribution on the cross-sectional area of the nanostructured and conventional TBCs after thermal shock testing were examined by a scanning electron microscope (SEM, KYKY−2800, Beijing, China), a field emission scanning electron microscope (FESEM, Sirion−200, Phillips, Netherlands) equipped with energy dispersive X-ray spectroscopy (GENESIS60S, EDAX Inc., USA), and the constituent phases of the top coat and spalled surfaces of the nanostructured and conventional TBCs were analyzed by a X-ray diffraction instrument (D/Max−2500, Rigaku, Japan), using Cu K_α radiation with wave-length of 1.540 51 Å.

3 Results and discussion

3.1 Thermal shock life at different test temperatures

Table 2 gives the results of thermal shock testing of the nanostructured and conventional TBCs. The experimental results indicate that the nanostructured TBC is superior to the conventional TBC. With increasing test temperature, the thermal shock life of nanostructured TBC decreases. As observed during the experiment, three was no macro-crack in the coating samples after 3 thermal cyclings. However, after 4 thermal cyclings, the edge of all samples started to spall, and surface cracks were observed by naked eyes. All of the coatings with substrate were bent toward the coating

side. This is because the volume of zirconia top coat decreases due to high temperature sintering and because the nickel substrate is only 2 mm thick that can be deformed.

The nanostructured TBC samples failed after 35 thermal cyclings at 1 150 ℃. All of the spalled surfaces were not white but green, regardless of test temperatures. This experimental result strongly indicates that the coating samples failed along the interface between the bond coat and substrate, rather than along the interface between the top coat and bond coat or in the ceramic top coat reported by other researchers[12].

3.2 Cracking modes and TBC failure

The cross-sectional micrographs of the nanostructured TBC failed after thermal shock testing at 1 150 ℃ are shown in Fig.1. These SEM micrographs were taken from the coating remained on the substrate. General view of the coating at a low magnification is shown in Fig.1(a). After 35 thermal cyclings at 1 150 ℃, more than 50% of the coating area was dropped, but obvious separation along the interface between the top coat and bond coat was not observed. Cracks formed in the zirconia top coat. Vertical cracks are clearly illustrated in Fig.1(b). The vertical cracks did not penetrate the whole top coat. They stopped in the area just above the top coat/bond coat interface. There appears to be a large horizontal crack in this area. However, under SEM at a high magnification (Fig.1(c)), it was found that it was not a real large horizontal crack. It was resulted from the breaking up of the zirconia top coat and pull out of the broken particles during grinding and polishing of the coating samples.

TGO formed in the bond coat of the nanostructured TBC tested at 1 150 ℃. Its thickness was about 2 μm. No small cracks formed at the crests of the undulated TGO layer (Fig.1(c)). TGO also formed at the bond coat/ substrate interface, but the TGO layer is not continuous

Table 2 Thermal shock test results of nanostructured and conventional TBCs

Cycling number	Nanostructured TBC			Conventional TBC
	1 150 ℃	1 200 ℃	1 250 ℃	1 250 ℃
3	Edge spalled	Edge spalled	Edge spalled	Edge spalled
4	Coating curved	Coating curved	Coating curved	Coating curved
5	Coating curved	Coating curved	Coating curved	Coating spalled
13	Coating curved	Coating curved	Coating spalled	
17	Coating curved	Coating spalled		
35	Coating spalled			

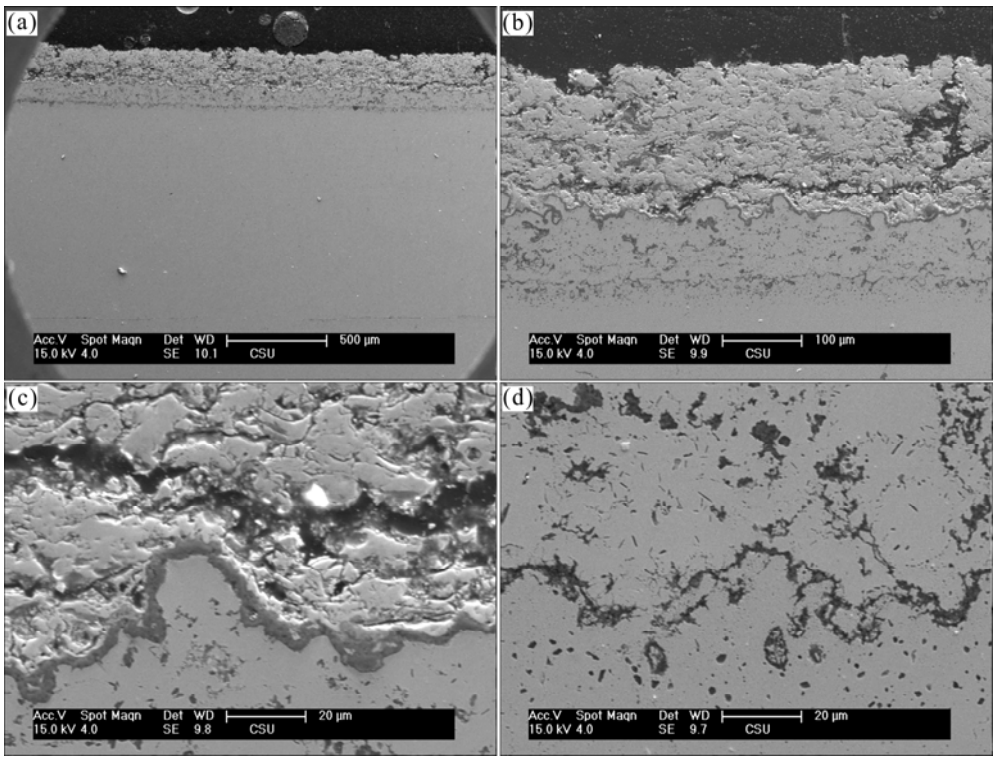

Fig.1 Cross-sectional micrographs of nanostructured TBC failed after 35 thermal cyclings at 1 150 ℃

(Fig.1(d)).

When thermal shock test was performed at 1 250 ℃, the nanostructured TBC failed only after 13 thermal cyclings. General view of the coating remained on the substrate is shown in Fig.2. It is seen from Fig.2(a) that the whole top coat appears no cracks. This results from the pull out of the broken particles during polishing of the sample. TGO thickness increases slightly, compared with that formed at 1 150 ℃. The number of large vertical cracks increases. However, these large vertical cracks did not penetrate the whole top coat (Fig.2(b)). Small cracks inside the so-called large horizontal crack were observed (Fig.2(c)), but small cracks in the top coat area just above the TGO layer were not observed. TGO formed at the bond coat/substrate interface and inside the bond coat (Fig.2(d)).

The thermal shock behavior of the conventional TBC was tested only at 1 250 ℃. Different from what was observed in the nanostructured TBC, large horizontal crack in the conventional TBC was not observed. However, large vertical cracks penetrated the whole top coat and stopped at the top coat/bond coat interface (Fig.3(a)). TGO formed at the interface with thickness of about 3 μm (Fig.3(b)). Unlike what happened in the nanostructured TBC, there was no breaking up of the conventional top coat and pull out of the particles during polishing of the sample. This experimental result tells us that the cohesive strength of conventional TBC is higher than that of nanostructured TBC.

3.3 Top coat phase stability

The monoclinic phase content in TBCs is important in predicting TBCs thermal shock performance. The lower the monoclinic phase content, the better the thermal shock performance of TBCs will be. X-ray diffraction patterns of the as-sprayed nanostructured TBC and the TBC samples after thermal shock testing at

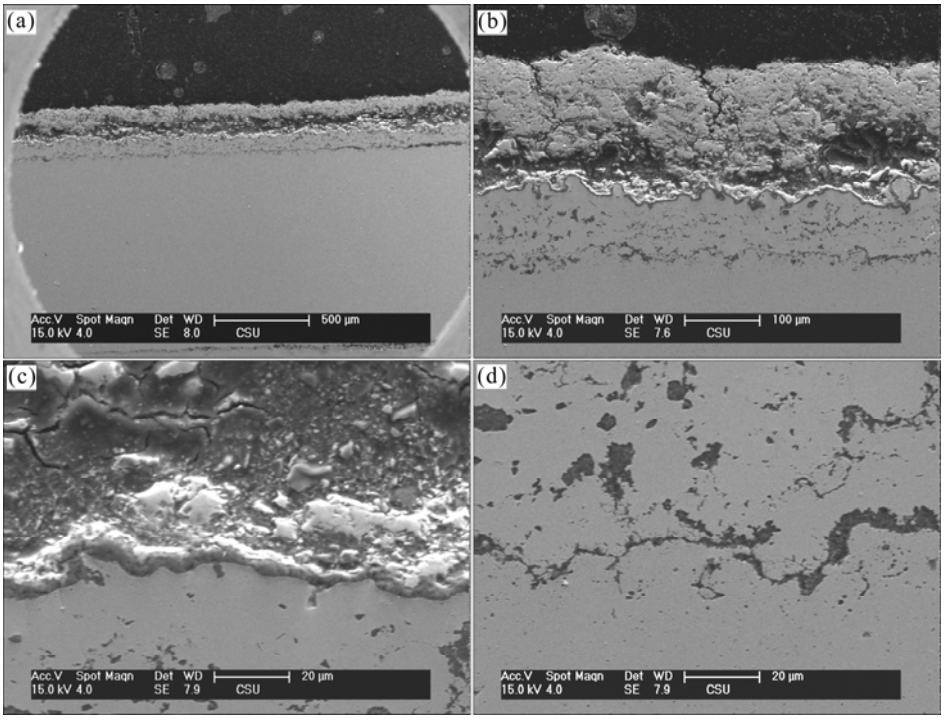

Fig.2 Cross-sectional micrographs of nanostructured TBC failed after 13 thermal cyclings at 1 250 ℃

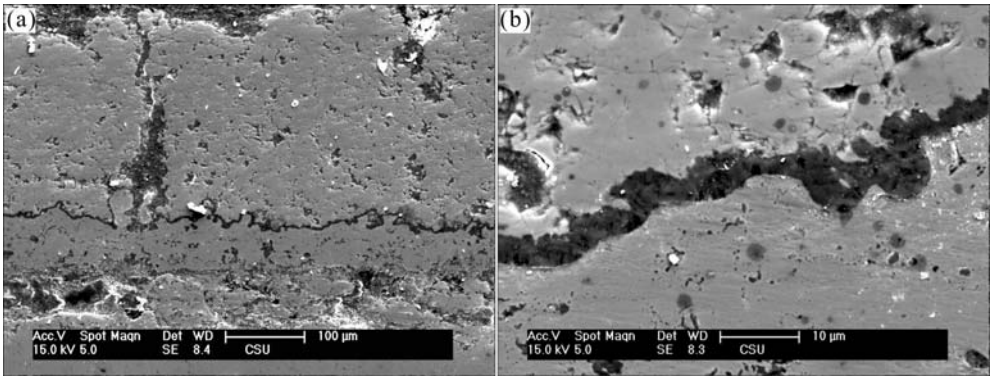

Fig.3 Cross-sectional micrographs of conventional TBC failed after 5 thermal cyclings at 1 250 ℃

1 150, 1 200, and 1 250℃ are shown in Fig.4. The as-sprayed nano-structured TBC is composed of cubic phase in accordance with PDF#30-1468. Composition of the cubic phase is Y0.15Zr0.85O1.93. After thermal shock testing at 1 150, 1 200 and 1 250 ℃, no obvious phase change was found.

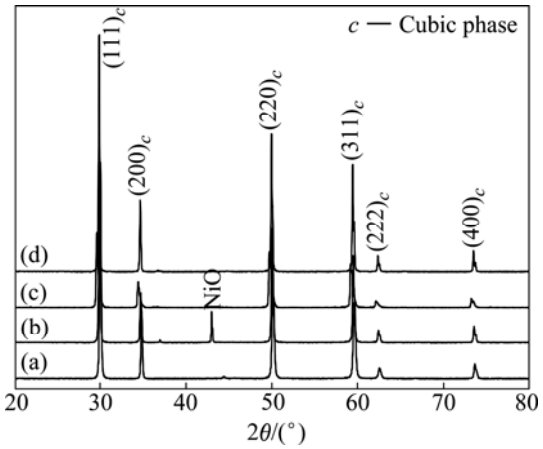

Fig.4 XRD patterns of nanostructured TBC before and after thermal shock testing at different temperatures: (a) As-sprayed; (b) 1 150℃; (c) 1 200 ℃; (d) 1 250 ℃

X-ray diffraction patterns of the as-sprayed conventional TBC and the TBC samples after thermal shock testing at 1 250 ℃ are shown in Fig.5. The as-sprayed conventional TBC is composed of diffusionless-transformed tetragonal (t') phase in accordance with PDF#48-0224. Composition of this phase is Y0.08Zr0.92O1.96. Phase transformation did not occur when thermal shock test was performed at 1 250 ℃. The XRD analysis result indicates that the diffusionless-transformed tetragonal phase did not decompose into equilibrium monoclinic phase and cubic phase under the experimental conditions.

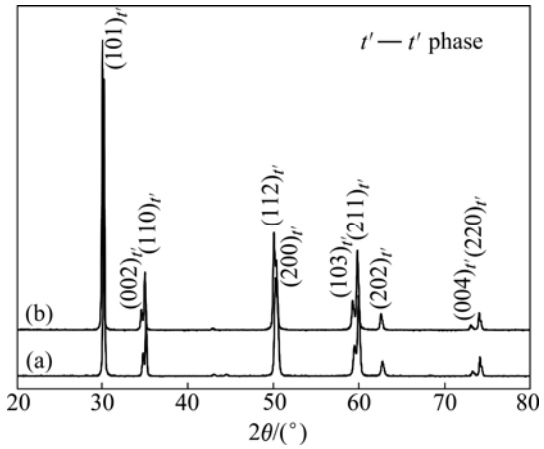

Fig.5 XRD patterns of conventional TBC: (a) As-sprayed; (b) After thermal shock testing at 1 250 ℃

3.4 Interface diffusion

The cross-sectional area elements scanning results of the nanostructured TBC after thermal shock testing at 1 150 and 1 250 ℃ are shown in Figs.6 and 7. It can be seen from Figs.6 and 7 that the diffusion of Al and O elements in the bond coat occurs. Al element diffuses from the bond coat toward the top coat/bond coat

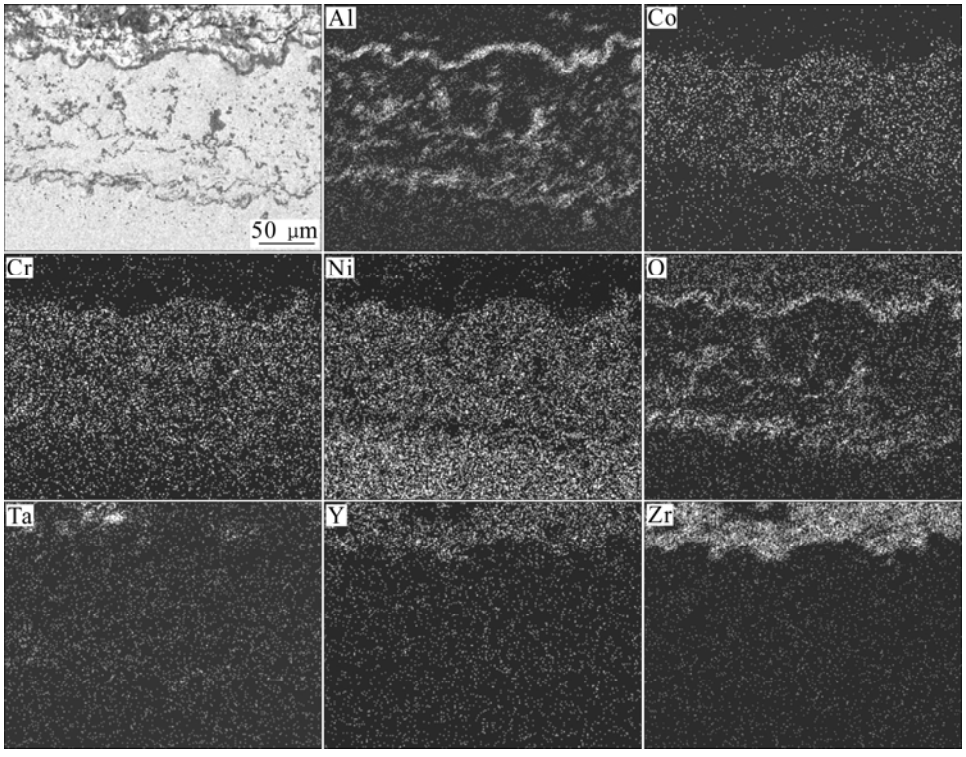

Fig.6 SEM micrograph and cross-sectional area scanning results of nanostructured TBC after thermal shock testing at 1 150 ℃

interface and O element diffuses through the top coat toward the bond coat and, as a result, Al_2O_3 formed at the interface. Inhomogeneous distributions of Al and O in the bond coat were observed from the area elements scanning pattern, indicating that Al_2O_3 also formed in the pore areas in the bond coat. Ni, Co, Cr and Ta are homogeneously distributed in the bond coat. The diffusions of Co, Cr, Al and Ta from the bond coat into the substrate are not evident when the temperature of thermal shock test is 1 250 ℃. Zr and Y in the ceramic top coat are stable.

The cross-sectional area elements distribution of the conventional TBC after thermal shock testing at 1 250 ℃ is shown in Fig.8. Al distribution in the bond coat is

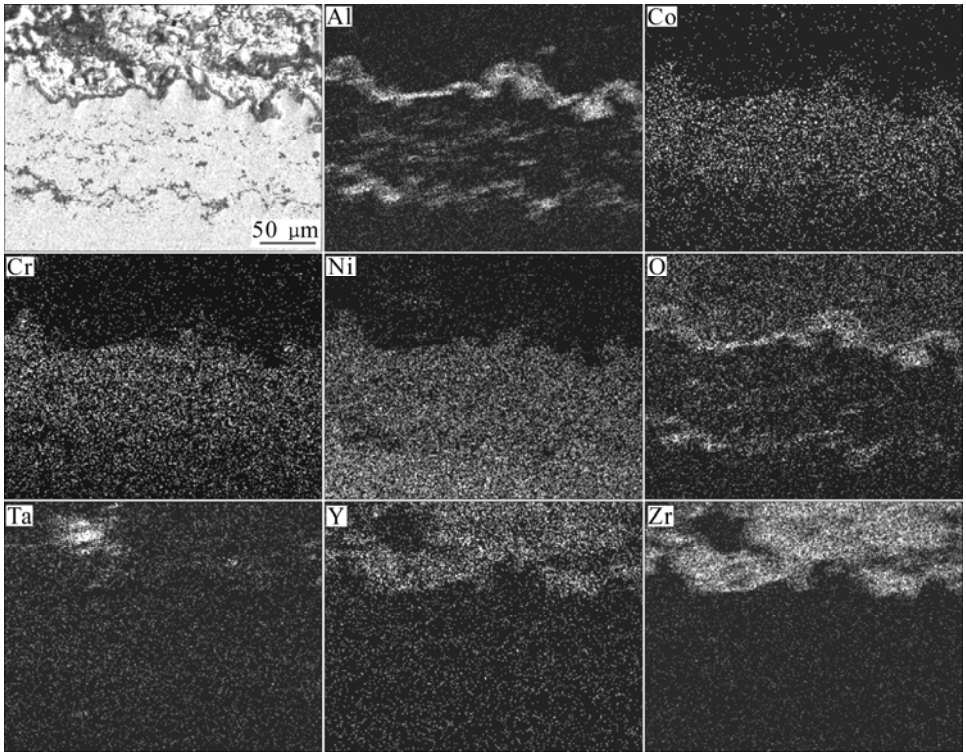

Fig.7 SEM micrograph and cross-sectional area scanning results of nanostructured TBC after thermal shock testing at 1 250 ℃

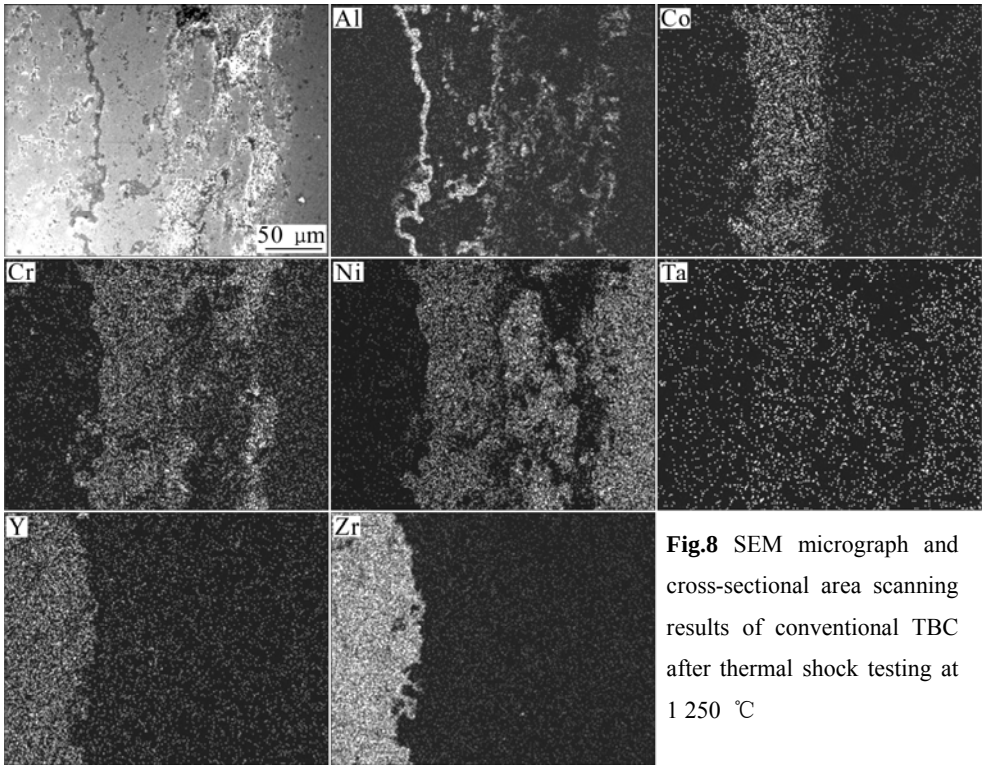

Fig.8 SEM micrograph and cross-sectional area scanning results of conventional TBC after thermal shock testing at 1 250 ℃

inhomogeneous. It concentrates at the top coat/bond coat interface where TGO forms. The inhomogeneous distribution of Al in the bond coat indicates that Al_2O_3 formed in the pore areas. Al and Cr were found on the surface layer of the Ni substrate.

3.5 Spallation along bond coat/substrate interface

SEM micrographs of the spalled surfaces of the nanostructured TBC after thermal shock testing at 1 150 and 1 250 ℃ are shown in Fig.9. These SEM micrographs were taken from the coating side. The spalled surfaces are rough and contain many large particles. These large particles consist of a bunch of small particles/crystals with different sizes. The size of the crystals formed at 1 250 ℃ is larger than that at 1 150 ℃. At 1 250 ℃, some crystals have grown to a few microns. The SEM micrographs of the spalled surface of the conventional TBC after thermal shock testing at 1 250 ℃ are shown in Fig.10. The average crystal size in the conventional TBC is larger than that in the nanostructured TBC although the test temperature is the same and total heating time is shorter. This phenomenon implies that the constituent phases in the spalled surfaces of the conventional and nanostructured TBCs could be different. In order to determine the constituent phases of the spalled surfaces, XRD was performed. XRD patterns are shown in Figs.11 and 12. The spalled surface of the nanostructured TBC contains $Ni_{2.88}Cr_{1.12}$, Al_2O_3, Cr_2O_3, $Ta_{0.8}O_2$ and $CoCr_2O_4$ at 1 150℃ and more Cr_2O_3 at 1 250 ℃. The $Ni_{2.88}Cr_{1.12}$ phase has the molar ratio of Ni to Cr close to the composition of the powder feedstock. These oxides form after oxygen diffuses into the bond coat/substrate interface during the thermal shock test. The formation of these oxides at the interface leads to the gradual loss of the bonding between the bond coat and nickel substrate, and final failure of the

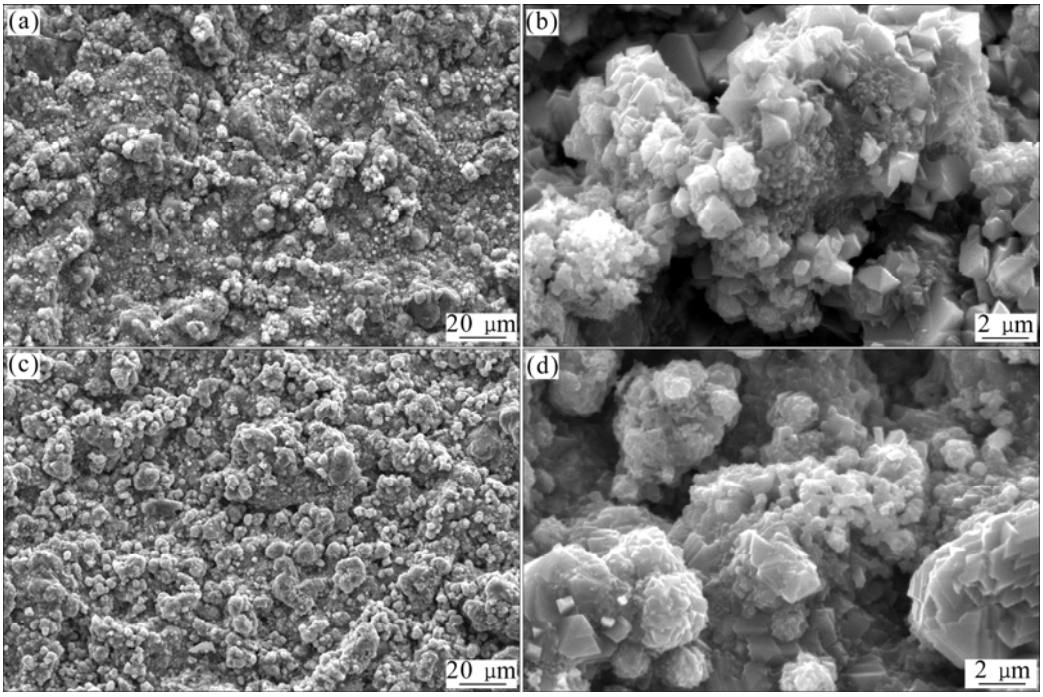

Fig.9 SEM micrographs of spalled surface of nanostructured TBC after thermal shock testing at 1 150 ℃ (a, b) and 1 250 ℃ (c, d)

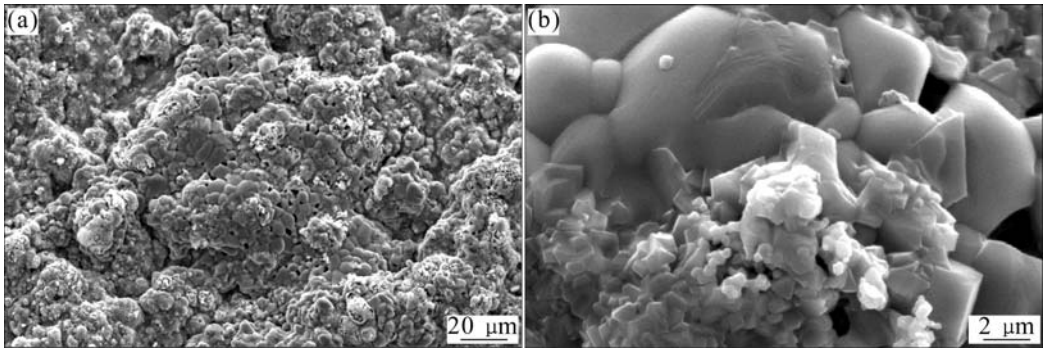

Fig.10 SEM micrographs of spalled surface of conventional TBC after thermal shock testing at 1 250 ℃

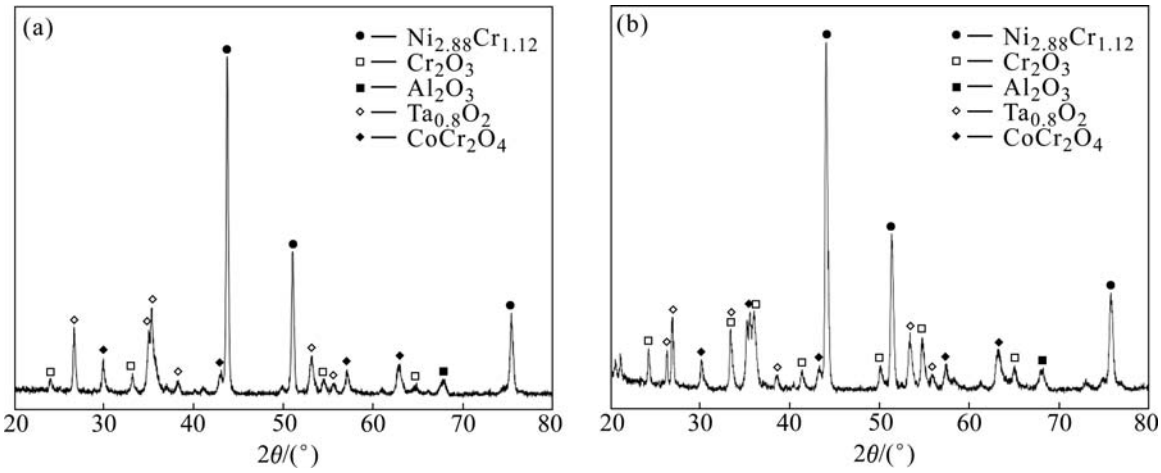

Fig.11 XRD patterns of spalled surfaces of nanostructured TBC after thermal shock testing at 1 150 ℃ (a) and 1 250 ℃ (b)

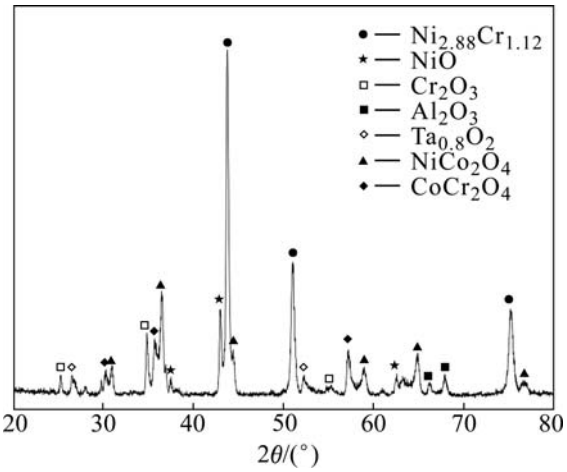

Fig.12 XRD pattern of spalled surface of conventional TBC after thermal shock testing at 1 250℃

TBC along this interface. In addition to $Ni_{2.88}Cr_{1.12}$, Al_2O_3, Cr_2O_3, $Ta_{0.8}O_2$ and $CoCr_2O_4$, the spalled surface of the conventional TBC tested at 1 250 ℃ contains NiO and $NiCo_2O_4$ but less Cr_2O_3. The NiO/$NiCo_2O_4$ at the bond coat/substrate interface may be the reason for explaining the crystal size difference in the spalled surfaces between the conventional and nanostructured TBCs.

No ZrO_2 diffraction peak in the XRD patterns shown in Figs.11 and 12 confirms the experimental observation that the nanostructured and conventional TBCs did not spall along the top coat/bond coat interface or in the ceramic top coat.

4 Conclusions

1) Nanostructured TBC is superior to conventional TBC in thermal shock performance. With increasing test temperature, the thermal shock life of nanostructured TBC decreases. Both nanostructured and conventional TBCs spalled at the bond coat/substrate interface after thermal shock testing.

2) The constituent phase of the as-sprayed conventional TBC is diffusionless-transformed tetragonal (t'). However, the constituent phase of the nanostructured TBC is cubic(c). After thermal shock testing, the constituent phases of both conventional and nanostructured TBCs did not change.

3) The diffusion of Al element at 1 150 and 1 250 ℃ is obvious while the diffusions of other bond coat elements are not evident. There is a difference in the crystal sizes at the spalled surfaces of the nanostructured and conventional TBCs. The constituent phases are composed of mainly $Ni_{2.88}Cr_{1.12}$ and oxides of bond coat elements.

References

[1] BELLE W, MARIJNISSEN G, LIESHOUT A V. The evolution of thermal barrier coatings status and upcoming solutions for today's key issues [J]. Surface and Coatings Technology, 1999, 120/121: 61−67.

[2] SCHULZ U, LEYENSA C, FRITSCHER K. Some recent trends in research and technology of advanced thermal barrier coatings [J]. Aerospace Science and Technology, 2003, 7(1): 73−80.

[3] LIU Chun-bo, LIN Feng, JIANG Xian-liang. Current state and future development of thermal barrier coating [J]. The Chinese Journal of Nonferrous Metals, 2007, 17(1): 1−13. (in Chinese)

[4] JIANG X L, LIU C B, LIN F. Overview on the development of nanostructured thermal barrier coatings [J]. Journal of Materials Science and Technology, 2007, 23(4): 440−456.

[5] LIMA R S, KUCUK A, SENTURK U, BERNDT C C. Integrity of nanostructured partially stabilized zirconia after plasma spray processing [J]. Materials Science and Engineering A, 2001, 313(1/2):

75−82.

[6] LIMA R S, KUCUK A, SENTURK U, BERNDT C C. Properties and microstructures of nanostructured partially stabilized zirconia coatings [J]. Journal of Thermal Spray Technology, 2001, 10(1): 150−152.

[7] CHEN H, DING C X. Nanostructured zirconia coatings prepared by atmospheric plasma spraying [J]. Surface and Coatings Technology, 2002, 150(1): 31−36.

[8] ZHOU C G, WANG N, WANG Z B. Thermal cycling life and thermal diffusivity of a plasma-sprayed nanostructured thermal barrier coating [J]. Scripta Materialia, 2004, 51(10): 945−948.

[9] LIANG B, DING C X. Microstructure of nanostructure zirconia coating and its thermal shock resistance [J]. Journal of Inorganic Materials, 2006, 21(1): 250−256.

[10] LIN Feng, YU Yue-guang, JIANG Xian-liang, ZENG Ke-li, REN Xian-jing, LI Zhen-duo. Microstructures and properties of nanostructured TBCs fabricated by plasma spraying [J]. The Chinese Journal of Nonferrous Metals, 2006, 16(3): 482−487. (in Chinese)

[11] SCHLICHTING K W, PADTURE N P, JORDAN E H, GELL M. Failure modes in plasma-sprayed thermal barrier coatings [J]. Materials Science and Engineering A, 2003, 342 (1/2): 120−130.

[12] LIANG B, DING C X. Thermal shock resistances of nanostructured and conventional zirconia coatings deposited by atmospheric plasma spraying [J]. Surface and Coatings Technology, 2005, 197(2/3): 185−192.

[13] NUSAIR KHAN A, LU J. Behavior of air plasma sprayed thermal barrier coatings subject to intense thermal cycling [J]. Surface and Coatings Technology, 2003, 166(1): 37−43.

[14] NUSAIR KHAN A, LU J. Thermal cyclic behavior of air plasma sprayed thermal barrier coatings sprayed on stainless steel substrates [J]. Surface and Coatings Technology, 2007, 201(8): 4653−4658.

[15] WANG W Q, SHA C K, SUN D Q, GU X Y. Microstructural feature, thermal shock resistance and isothermal oxidation resistance of nanostructured zirconia coating [J]. Materials Science and Engineering A, 2006, 424(1/2): 1−5.

[16] SHUI Y, ZHANG P C, JIANG C, WANG S G, XIAO Y F. Study on fabrication of zirconia nanopowder plasma sprayed coating [J]. Transactions of Materials and Heat Treatment, 2004, 25(1): 17−20.

[17] LU Y H, WANG Q S, WU Z J. Thermal shock resistance of plasma sprayed nanostructured ZrO_2 thermal barrier coating [J]. Journal of Materials Protection, 2006, 39(7): 9−12.

[18] ZHOU C G, WANG N, XU H B. Comparison of thermal cycling behavior of plasma sprayed nanostructured and traditional thermal barrier coatings [J]. Materials Science and Engineering A, 2007, 452/453: 569−574.

(Edited by YANG Bing)